Dynamics and Rheology of Vesicle Suspensions in Wall-Bounded Shear Flow

Antonio Lamura[1] [(a)] and Gerhard Gompper[2] [(b)]

[1] *Istituto Applicazioni Calcolo, CNR, Via Amendola 122/D, 70126 Bari, Italy*
[2] *Theoretical Soft Matter and Biophysics, Institute of Complex Systems, Forschungszentrum Jülich, 52428 Jülich, Germany*

PACS 87.16.D- – Membranes, bilayers, and vesicles
PACS 83.80.Lz – Rheology: Physiological materials (e.g. blood, collagen, etc.)
PACS 87.17.Aa – Theory and modeling; computer simulation

Abstract – The dynamics and rheology of suspensions of fluid vesicles or red blood cells is investigated by a combination of molecular dynamics and mesoscale hydrodynamics simulations in two dimensions. The vesicle suspension is confined between two no-slip walls, which are driven externally to generate a shear flow with shear rate $\dot{\gamma}$. The flow behavior is studied as a function of $\dot{\gamma}$, the volume fraction of vesicles, and the viscosity contrast between inside and outside fluids. Results are obtained for the encounter and interactions of two vesicles, the intrinsic viscosity of the suspension, and the cell-free layer near the walls.

Introduction. – Suspensions of mesoscale particles in viscous liquids are ubiquitous, with examples in biological systems (blood flow), home products (paints), food products (emulsions), and industrial processing (pastes). The suspended particles can be spheres, rods, fibers, flexible and semiflexible macromolecules, droplets, capsules, vesicles and cells. While the dynamics of rigid particles in suspension and their rheological behavior have been investigated in considerable detail and are by now reasonably well understood [1], much less is known about the dynamics and rheology of *deformable* particles, in particular in the semi-dilute regime, where hydrodynamic and steric interactions between the particles become important.

The dynamics of soft objects, in particular under flow, depends on the physical origin of their deformability, like the surface tension at constant volume for droplets, the membrane bending rigidity at fixed volume and surface area for vesicles, and in addition the membrane shear elasticity for capsules and cells. Therefore, these systems have to be investigated independently to understand the relation between the elasticity of the particles and the rheological behavior of their suspensions.

In the dilute regime, the vesicle dynamics shows tank-treading (TT), tumbling (TU) and vacillating-breathing dynamics, depending on shear rate $\dot{\gamma}$ and viscosity contrast λ [2–8]. For TT quasi-spherical vesicles in three dimensions (3D), the viscosity of a dilute suspension has been predicted to be [9,10]

$$\eta/\eta_{out} = 1 + \frac{5}{2}\,\phi\left[1 - \frac{\Delta}{40\pi}(23\lambda + 32)\right] \qquad (1)$$

as a function of excess area $\Delta = 4\pi[\frac{A}{4\pi}(\frac{4\pi}{3V})^{2/3} - 1]$ and viscosity contrast $\lambda = \eta_{in}/\eta_{out}$, where A and V are the surface and volume of the vesicle, η_{in} and η_{out} are the fluid viscosities of the inner and outer fluids, respectively, and ϕ is the vesicle volume fraction. Thus, the intrinsic viscosity $\eta_I = (\eta - \eta_{out})/(\eta_{out}\phi)$ is predicted to be a decreasing function of Δ and λ. Furthermore, η_I is foreseen to have a cusp-like minimum at the tank-treading to tumbling (or tank-treading to vacillating-breathing) transition, and then to increase again with increasing λ [9,10]. This latter behavior has been also found in the numerical calculations of a two-dimensional vesicle by the boundary-integral approach [11].

These theoretical predictions have been tested experimentally [12,13]. While a decrease of η_I with increasing λ was found in ref. [12], in good agreement with the theoretical prediction (1), in contrast an increase of η_I was found in ref. [13]. However, the available experimental results are not conclusive for several reasons. First, vesicle sizes

[(a)] E-mail: a.lamura@ba.iac.cnr.it
[(b)] E-mail: g.gompper@fz-juelich.de

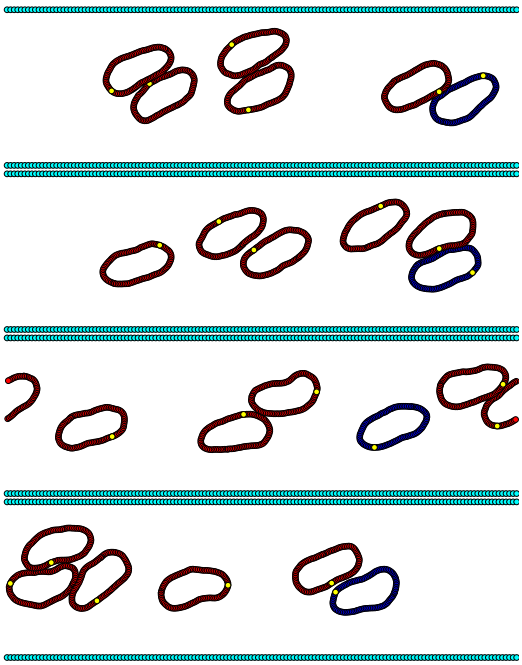

Fig. 1: Configurations at consecutive times $\dot{\gamma}t = 424$, 440, 456, 472 (from top to bottom) of vesicles with viscosity contrast $\lambda = 1.0$, reduced area $A^* = 0.8$, reduced shear rate $\gamma^* = 2.0$, and concentration $\phi = 0.14$. One vesicle is colored blue for better visualisation of its evolution during tank-treading. See also movie S1 for $\lambda = 2.0$, $A^* = 0.8$, $\gamma^* = 2.0$, and $\phi = 0.28$.

in suspensions are typically polydisperse. Second, viscosity measurements require a minimum volume fraction ϕ of vesicles, typically 5% to 10%, and are therefore difficult to extrapolate to the dilute limit [13]. Indeed, experiments have been performed recently [14] which demonstrate that vesicle interactions become relevant for the viscosity for ϕ around 10%.

Therefore, we study here the rheology of vesicle suspensions in the "semi-dilute" regime, where particle interactions are important, but particles are not yet densely packed into a glassy state. Our results are obtained from mesoscale hydrodynamics simulations of two-dimensional (2D) model systems, which allow the study of larger system sizes and longer time scales. Compared to the theory of ref. [9, 10] and the simulations of ref. [11], our model includes thermal fluctuations and has the capability of studying systems over a wide range of vesicle concentrations. Our main results concern the dependence of the intrinsic viscosity on viscosity contrast, shear-thinning behavior, displacements and angular oscillations in two-vesicle collisions, and the dependence of cell-free-layer thickness on shear rate $\dot{\gamma}$.

Method and Model. – Each vesicle in two dimensions is modeled as a chain of N_p beads of mass m_p, connected successively in a closed ring [15], see fig. 1. Neighboring beads are connected to each other by an harmonic potential with spring constant k_h and average bond length r_0; this keeps the perimeter length of the membrane constant, both locally and globally. Shapes and fluctuations are then controlled by a bending potential $V_b = (\kappa/r_0)\sum_i(1-\cos\beta_i)$, where β_i is the angle between the two bond vectors at bead i, and κ is the bending rigidity. Finally, in order to keep the vesicle area A close to the target value A_0, a potential $V_A = k_A(A-A_0)^2/(2r_0^4)$ is employed, where k_A is the compression modulus. Different vesicles repel each other at short distances via a shifted Lennard-Jones potential, which is truncated at its minimum r_{cut}. Newton's equations of motions for the beads are integrated by using the velocity-Verlet algorithm with time step Δt_p [16].

The fluid is described by multi-particle collision (MPC) dynamics, a particle-based mesoscale simulation technique [17–19]. The two-dimensional fluid consists of N_s point particles of mass m, whose positions $\mathbf{r}_i(t)$ and velocities $\mathbf{v}_i(t)$, $i = 1, 2, ..., N_s$, are continuous variables. The evolution occurs in discrete time intervals Δt_s, and proceeds in two consecutive steps: streaming and collision. In the streaming step, particles move ballistically. In the collision step, the particles are sorted into the cells of a regular square lattice of mesh size a; all particles within each cell collide and exchange momentum. We employ here a variant of MPC, denoted as MPC-AT+a, which conserves both linear and angular momentum locally [20, 21] and keeps the temperature constant [20]. The viscosity of the MPC-AT+a fluid in two dimensions is given by

$$\eta = \frac{m}{\Delta t_s}\Big[\Big(\frac{l}{a}\Big)^2\Big(\frac{n^2}{n-1}-\frac{n}{2}\Big)+\frac{1}{24}\Big(n-\frac{7}{5}\Big)\Big] \qquad (2)$$

with $l = \Delta t_s\sqrt{k_BT/m}$ the mean-free path, k_BT the thermal energy, and n the average number of particles per cell [22]. The system of size $L_x \times L_y$ is placed between two horizontal walls which slide along the x direction with velocities v_{wall} and $-v_{wall}$, respectively. Periodic boundary conditions are used along the x direction. A bounce-back rule with virtual particles ensures no-slip boundary conditions at the walls [21, 23]. This generates a linear flow profile $v_x = \dot{\gamma}y$ with shear rate $\dot{\gamma} = 2v_{wall}/L_y$.

To describe the fluid-membrane interaction, membrane beads are modeled as hard disks, see fig. 1. The radius r_p of the disks is chosen large enough to ensure mutual overlap and a complete coverage of the membrane to prevent fluid particles from crossing the membrane. Since it is very important to conserve linear and angular momentum for vesicles with viscosity contrast [21, 24], we employ the following scattering rule between fluid particles and membrane disks. Scattering occurs only when a fluid particle j and a membrane disk i overlap and move towards each other, so that the conditions $|\mathbf{r}_i - \mathbf{r}_j| < r_p$ and $(\mathbf{r}_i - \mathbf{r}_j)\cdot(\mathbf{v}_i - \mathbf{v}_j) < 0$ are satisfied. A second disk $k = i \pm 1$ in the same membrane, with $\min_{k=i\pm1}|\mathbf{r}_k - \mathbf{r}_j|$, is selected to perform a three-body collision which conserves linear and angular momenta [24]. The MPC collision step is then performed only for those fluid particles which did

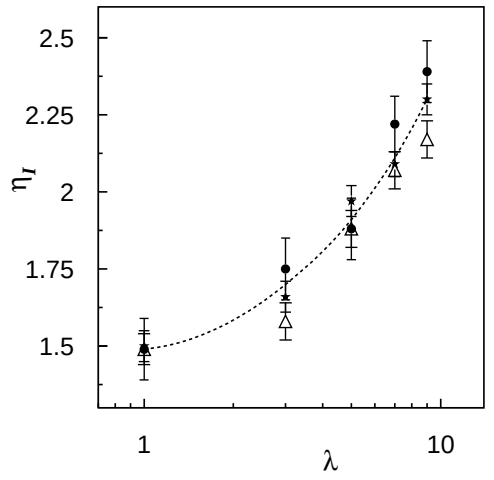

Fig. 2: The intrinsic viscosity $\eta_I = (\eta - \eta_{out})/(\eta_{out}\phi)$ as a function of the viscosity contrast λ for reduced shear rate $\gamma^* = 2.0$, reduced area $A^* = 0.8$, and concentrations $\phi = 0.05$ (•), 0.09 (△), and 0.14 (⋆). The dashed line is the interpolation to the data (⋆). The tank-treading-to-tumbling transition occurs at $\lambda_c \simeq 3.7$ for $A^* = 0.8$ in the KS theory [2].

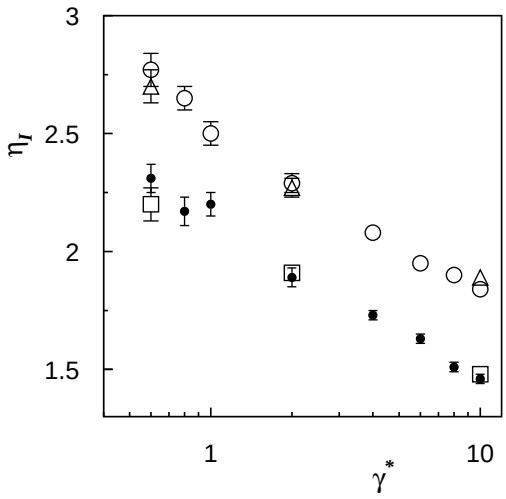

Fig. 3: The intrinsic viscosity $\eta_I = (\eta - \eta_{out})/(\eta_{out}\phi)$ as a function of the reduced shear rate γ^* for reduced area $A^* = 0.8$, concentration $\phi = 0.28$, and viscosity contrasts $\lambda = 2.0$ (•) and 5.0 (○) with $L_x \times L_y = (18.95 \times 5.79)R_0$, and $\lambda = 2.0$ (□) and 5.0 (△) with $L_x \times L_y = (15.79 \times 6.84)R_0$. When not visible, error bars are comparable with symbols size.

not participate in the membrane scattering, in order to avoid multiple collisions with the same disk in subsequent time steps. The fluids in the interior and exterior of the vesicle may differ in their particle mass to control viscosity. Membrane disks interact with walls via bounce-back.

In experiments with vesicles in shear flow, inertial effects are negligible since the Reynolds number $Re = \dot{\gamma}\rho R_0^2/\eta_{out}$, where $\rho = nm/a^2$ is the fluid mass density, is typically very small. We express the results in dimensionless quantities, such as the reduced area $A^* = A_0/\pi R_0^2$ (where $R_0 = L_0/(2\pi)$ is the mean vesicle radius with membrane length L_0) and the reduced shear rate $\gamma^* = \dot{\gamma}\eta_{out}R_0^3/\kappa$. We set $n = 10$, $l_{out} = 0.0064a$ with $l_{in} = l_{out}\sqrt{m_{out}/m_{in}}$ (in the following the subscripts out/in will refer to quantities outside/inside of the vesicle). This implies that the viscosity contrast is $\lambda = \eta_{in}/\eta_{out} \simeq m_{in}/m_{out}$. We use the system size $L_x = 18.95R_0$, $L_y = 5.79R_0$, mean radius $R_0 = 7.6a$, and v_{wall} such that $Re < 0.2$ for all the cases we considered with $0.4 \leq \gamma^* \leq 10.0$. Finally, we set m_{in} such that $0.1 \leq \lambda \leq 13.0$, $m_p = 3m_{out}$, $N_p = 480$, $\Delta t_p = \Delta t_s/64$, $r_p = r_0 = a/10$, $r_{cut} = a$, $\kappa = 6.58k_BTR_0$, $k_A = 4 \times 10^{-4}k_BT$, $k_h = 3 \times 10^2 k_BT$, and A_0 such that $0.8 \leq A^* \leq 0.95$. This value of κ gives rise to a similar amplitude of undulation modes as for lipid bilayer membranes in 3D (where $\kappa_{3D} \simeq 10k_BT$). With these choices for k_A and k_h, the area and the length of the vesicle are kept constant with a deviation less than 1% of the target values for all simulated systems.

Results. –

Suspension Viscosity. We first consider dilute and semi-dilute monodisperse suspensions of vesicles with fixed reduced shear rate $\gamma^* = 2.0$. Systems with $N_V = 2$, 4, or 6 vesicles are studied, corresponding to concentrations $\phi = 0.05$, 0.09, and 0.14, for different viscosity contrasts λ. A few typical vesicle configurations for $\phi = 0.14$ and $\lambda = 1.0$ are displayed in fig. 1. The suspension viscosity η is calculated numerically [25] from the component σ_{xy} of the stress tensor, so that $\eta = \sigma_{xy}/\dot{\gamma}$ [1].

The relative viscosity $(\eta - \eta_{out})/\eta_{out}$ is a linear function of ϕ for $A^* = 0.8$ and various values of λ as predicted by the Einstein relation [26]. In fig. 2, the intrinsic viscosity η_I is shown as a function of λ for various concentrations with $A^* = 0.8$. An increase of η_I with the viscosity contrast is observed. We do not find an indication of a non-monotonic behavior — as predicted theoretically by eq. (1) in refs. [9,10] for quasi-spherical vesicles in 3D and obtained numerically in 2D in ref. [11] — in the explored range $1.0 \leq \lambda \leq 9.0$ of viscosity contrasts, although the dynamic behavior changes from TT to TU at intermediate values of λ. In two dimensions, the TT-to-TU transition is predicted to occur at $\lambda_c \simeq 3.7$ for $A^* = 0.8$ in the Keller-Skalak (KS) theory [2]. However, thermal vesicle undulations, which are neglected in KS theory, produce a continuous crossover from TT to TU for bending rigidities around $\kappa = 6.4k_BTR_0$ [24], with $A^* = 0.7$ and $\gamma^* \lesssim 6$. Thus, our simulation results of increasing $\eta_I(\lambda)$ are in qualitative agreement with the experimental results of ref. [13] for semi-dilute systems.

We consider next the behavior of monodisperse concentrated suspensions with $\phi = 0.28$ (12 vesicles) with reduced area $A^* = 0.8$ for viscosity contrasts $\lambda = 2.0$, 5.0 as a function of the reduced shear rate γ^*. Two systems of size $L_x \times L_y = (18.95 \times 5.79)R_0$ and $(15.79 \times 6.84)R_0$ are investigated, which have the same area but the latter being a vesicle radius R_0 wider than the former. The results of the intrinsic viscosity η_I are displayed in fig. 3. The

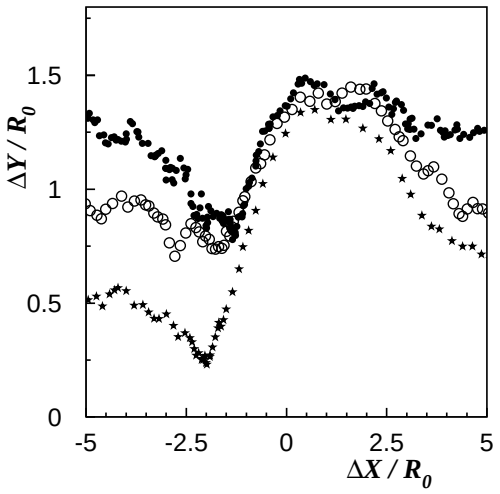

Fig. 4: Relative vertical displacement of the centers of mass $\Delta Y/R_0$ of two scattering vesicles with respect to the relative horizontal distance $\Delta X/R_0$ for $\lambda = 1.0$, $A^* = 0.8$, and shear rates $\gamma^* = 2.0$ (•), 5.0 (○), and 10.0 (⋆).

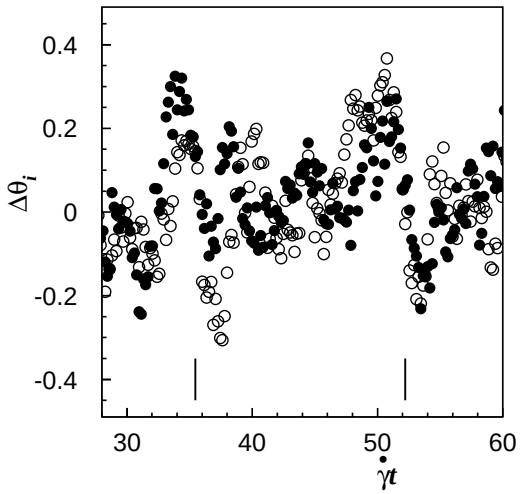

Fig. 5: Dynamics of two vesicles over two subsequent interaction events. Deviations $\Delta\theta_i$ of the inclination angles of both the two vesicles ($i = 1, 2$, indicated by the two types of symbols) from the average stationary value are shown as a function of time for the run in fig. 4 with $\gamma^* = 2.0$. The vertical lines denote the times of the closest relative distance between the two vesicles. See also movie S2, which displays vesicle interactions in the time range $30 < \dot{\gamma}t < 60$.

values of η_I are not affected by the system size. For both values of λ, a significant shear-thinning behavior is found over more than one decade in the reduced shear rate. The data also show that it is difficult to reach the low shear-rate plateau in simulations. This is due to the importance of thermal motion at low shear rates, but may also be related to the broad TT-to-TU transition in 2D [24] where some tumbling events already appear in the TT regime. This shear-thinning is mainly due to the formation of cell-free layers near the walls, as expected from the Fåhraeus-Lindqvist effect [27]. The formation of cell-free layers will be discussed in detail below. An analysis of the effective viscosity in the central part of the channel, as derived from the local shear rate, shows that shear-thinning of the core region, as observed in bulk red blood cell suspensions in 3D, both experimentally [28] and in simulations [29], is not significant in 2D in the considered concentration range.

Vesicle Interactions. Following the experimental work in refs. [13,14], we study the interaction between two vesicles with $A^* = 0.8$ in the TT regime ($\lambda = 1.0$). Figure 4 displays the relative vertical displacement of the centers of mass $\Delta Y = y_{cm1} - y_{cm2}$ during scattering with respect to the horizontal displacement $\Delta X = x_{cm1} - x_{cm2}$, where (x_{cm1}, y_{cm1}) and (x_{cm2}, y_{cm2}) are the positions of the centers of mass of the two vesicles, for three different shear rates $\gamma^* = 2.0$, 5.0, and 10.0. Movie S2 illustrates the vesicle interaction for $\gamma^* = 2.0$. Figure 4 shows four important effects: (i) When the vesicles are released from their initial positions in the upper and lower halves of the channel, they migrate towards the center due to the wall-induced lift force ($\Delta X/R_0 \lesssim -2$); (ii) upon collision, the vesicles are displaced and reach a maximum in their vertical separation ΔY corresponding to the small vesicle diameter ($\Delta X/R_0 \simeq 0$); (iii) immediately after the collision, the vertical displacement is larger than before the collision ($\Delta X/R_0 \simeq 2.5$); (iv) the vesicle continue to migrate towards the center line ($\Delta X/R_0 \gtrsim 2.5$). Different shear rates mainly determine the migration rate, but seem to have little effect on the collision process itself. Good agreement for the collision process is found with experimental results, which are obtained for much wider channels (see fig. 2 of ref. [13]). The increased vertical separation after scattering is in qualitative agreement with recent theoretical predictions for quasi-spherical vesicles and large inter-vesicle distances [30].

The interaction process can also monitored in time by considering the behavior of the distance d between the centers of mass of the vesicles and the deviations $\Delta\theta_i = \theta_i - \theta_0$ of the inclination angle θ_i ($i = 1, 2$) of the two vesicles from its average stationary value θ_0. This latter is shown in fig. 5 for two consecutive scattering events for the same run of fig. 4 with reduced shear rate $\gamma^* = 2.0$. We observed a correlation of the tilt angles of the vesicles when the relative distance is at minimum, in agreement with the experimental results (compare with fig. 8 of ref. [14]). In fig. 6, the deviations $\Delta\theta_i$ are shown as a function of the relative displacement angle α, defined as the angle between the direction along the vesicles centers of mass and the flow direction, for the run in fig. 4 with $\gamma^* = 2.0$. Data are averaged over four subsequent scattering processes. The maximum and minimum of $\Delta\theta_i$ occur approximately at $\alpha \simeq 3\pi/4$ and $\alpha \simeq \pi/4$, corresponding to the compression and stretching directions of the shear flow field, respectively. This is again in agreement with the recent experimental results (see fig. 6 of ref. [14]), except for a small displacement of the minimum position.

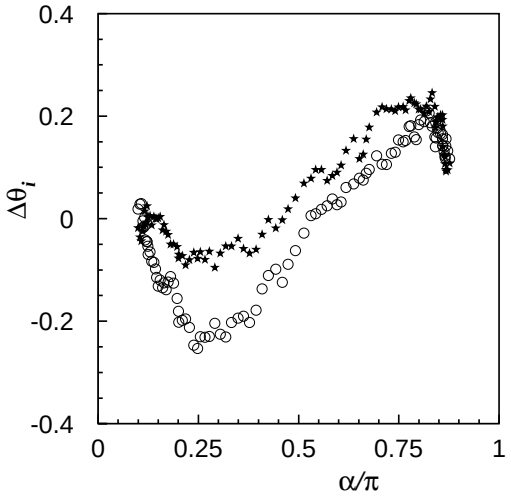

Fig. 6: Deviations $\Delta\theta_i$ of the inclination angles of two interacting vesicles ($i = 1, 2$, indicated by the two types of symbols) from the average stationary value as a function of α, the angle between the direction connecting the vesicles centers of mass and the flow direction, for the run in fig. 4 with $\gamma^* = 2.0$. Data are averaged over four subsequent interaction events.

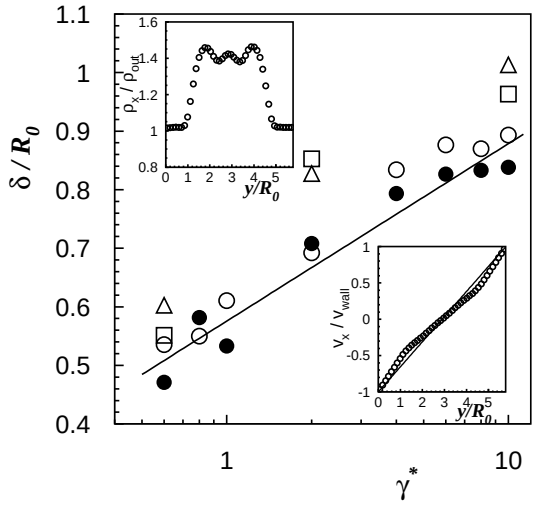

Fig. 7: The ratio of the average thickness δ of the vesicle-free boundary layers to the vesicle radius R_0 as a function of the reduced shear rate γ^* for reduced area $A^* = 0.8$, concentration $\phi = 0.28$, and viscosity contrasts $\lambda = 2.0$ (•) and 5.0 (○) with $L_x \times L_y = (18.95 \times 5.79)R_0$, and $\lambda = 2.0$ (□) and 5.0 (△) with $L_x \times L_y = (15.79 \times 6.84)R_0$. Error bars are comparable with symbols size. The full line is a logarithmic fit to data points (•). Insets: (left) Fluid mass density and (right) fluid velocity component v_x, averaged along the flow (x) direction, both across the channel with $\lambda = 2.0$ and $\gamma^* = 10.0$. (Right) The full line corresponds to the imposed shear flow profile.

Cell-Free Boundary Layer. For red blood cells (RBCs) in capillary flow, it was first found by Fåhraeus and Lindqvist [27] that cells are depleted from a layer near the vessel wall. It is now well understood that this is a consequence of the wall-induced hydrodynamic lift force on the cells [24]. For concentrated systems with $\phi = 0.28$, we have measured the average thickness δ of the cell-free boundary layers near the walls. δ is defined as the time average of $(d_1(t) + d_2(t))/2$ with $d_{1,2}(t) = \min_{i=1,\ldots,N_V} l_i(1,2)(t)$, where N_V is the number of vesicles and $l_i(1,2)$ the closest distance of i-th vesicle membrane from either of the two walls. The results are reported in fig. 7 as a function of the reduced shear rate. The ratio δ/R_0 increases with γ^* for both the values of the considered viscosity contrasts. The data are consistent with a logarithmic growth of δ with increasing γ^*. With increasing system width, the values of δ grow, as also observed in two-dimensional simulations of RBC-like vesicles in capillary flow [31].

The existence of boundary layers is also supported by considering the fluid mass density profiles in the steady state averaged along the flow direction x. The mass density is lower in the cell-free boundary layers at the walls due to the absence of vesicles with a heavier fluid inside (see the inset of fig. 7). This effect of the boundary layer is also evident in steady-state velocity profiles, which display a smaller effective shear rate in the center and a higher shear rate near the wall, as compared to the imposed shear rate $\dot{\gamma}$ (see the inset of fig. 7).

Finally, the behavior of δ as a function of λ for $\gamma^* = 2.0$ is shown in fig. 8 for the two system sizes. It is evident that there is a pronounced non-linear dependence of δ on λ, with the boundary layer decreasing at high values of the viscosity contrast, attaining a maximum near the TT-to-TU transition. This behavior can be related to the dependence of the lift force on the viscosity contrast, which has been shown [24] to be a decreasing function of λ. In the TT phase, the increase of δ might be due to the reduction of the tilt angle with increasing λ, which facilitates the sliding of vesicles past each other and allows them to be squeezed more easily into the center of the channel. In the TU phase, tumbling of vesicles is suppressed near the wall, which further reduces the lift force [24].

The cell-free layer thickness δ is found to grow with L_y, in agreement with simulations of RBCs in cylindrical microchannels in 3D (compare fig. 10 of ref. [32]). δ is found to increase with $\dot{\gamma}$, in agreement with the results of RBC simulations in 3D presented in fig. 8 of ref. [33], but at odds with the simulation results in fig. 11 of ref. [32] and experimental results of ref. [34]. This apparent discrepancy can be partially resolved by taking a closer look at the investigated range of shear rates. In our 2D case, the increase of δ occurs for $\gamma^* \lesssim 7$; in ref. [33], it is seen for $\gamma^* \lesssim 20$ in 3D; and in ref. [32], δ is found to slightly decrease for $\gamma^* \gtrsim 4$ (in refs. [32, 33] the average shear rate is used, computed from the average velocity in a Poiseuille flow; for RBCs in three dimensions, we use $\tau = \eta_0 R_0^3/\kappa$ with mean radius $R_0 = 3.4\mu$m, bending rigidity $\kappa = 50 k_B T$, and the plasma viscosity $\eta_0 = 0.0012$ Pa s — which implies $\tau = 0.22$ s — to determine the dimensionless shear rate). Although it is of course difficult to compare results

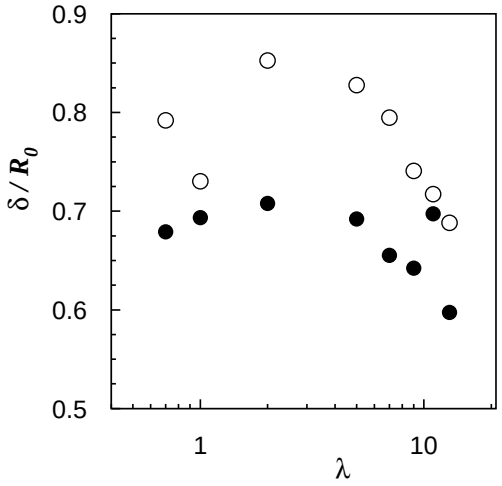

Fig. 8: The ratio of the average thickness δ of the vesicle-free boundary layers to the vesicle radius R_0 as a function of the viscosity contrast λ for reduced area $A^* = 0.8$, reduced shear rate $\gamma^* = 2.0$, concentration $\phi = 0.28$, and system sizes $L_x \times L_y = (18.95 \times 5.79)R_0$ (•) and $L_x \times L_y = (15.79 \times 6.84)R_0$ (○). Error bars are comparable with symbols size.

of 2D and 3D systems quantitatively, we can conclude that there is a critical reduced shear rate $\gamma_c^* \simeq 10$ below which δ is increasing with γ^*, and above which δ is constant or slowly decreasing. The value of γ_c^* depends, of course, on the channel width and the vesicle volume fraction [32]; the value above should be valid for volume fractions around 0.3 and channel widths of about three vesicle diameters.

Summary and Conclusions. – We have investigated the dynamical behavior of semi-dilute suspensions of vesicles or red blood cells under shear flow in a narrow gap between two walls. The advantage of the Couette geometry compared to Poiseuille flow is that wall effects and effects of a non-linear flow profile do not interfere. We find the intrinsic viscosity to increase monotonically with increasing viscosity contrast, a pronounced shear-thinning behavior with increasing shear rate due to the Fåhraeus-Lindqvist effect, displacements and angular oscillations in two-vesicle collisions in good agreement with experiments, and an increase of the cell-free-layer thickness with shear rate $\dot{\gamma}$ below a critical reduced shear rate $\gamma_c^* \simeq 10$.

* * *

Fruitful discussions with D. Fedosov, I. O. Götze, S. Messlinger, H. Noguchi, and M. Peltomaeki are gratefully acknowledged.

REFERENCES

[1] Mewis J. and Wagner N. J., (Editors) *Colloidal Suspension Rheology* (Cambridge University Press, Cambridge) 2012.
[2] Keller S. R. and Skalak R., *J. Fluid Mech.* , **120** (1982) 27.
[3] Kantsler V. and Steinberg V., *Phys. Rev. Lett.* , **95** (2005) 258101.
[4] Kantsler V. and Steinberg V., *Phys. Rev. Lett.* , **96** (2006) 036001.
[5] Misbah C., *Phys. Rev. Lett.* , **96** (2006) 028104.
[6] Noguchi H. and Gompper G., *Phys. Rev. Lett.* , **98** (2007) 128103.
[7] Lebedev V. V., Turitsyn K. S. and Vergeles S. S., *Phys. Rev. Lett.* , **99** (2007) 218101.
[8] Vlahovska P. M. and Gracia R. S., *Phys. Rev. E* , **75** (2007) 016313.
[9] Danker G. and Misbah C., *Phys. Rev. Lett.* , **98** (2007) 088104.
[10] Danker G., Biben T., Podgorski T., Verdier C. and Misbah C., *Phys. Rev. E* , **76** (2007) 041905.
[11] Ghigliotti G., Biben T. and Misbah C., *J. Fluid Mech.* , **653** (2010) 489.
[12] Vitkova V., Mader M.-A., Polack B., Misbah C. and Podgorski T., *Biophys. J.* , **95** (2008) L33.
[13] Kantsler V., Segre E. and Steinberg V., *EPL* , **82** (2008) 58005.
[14] Levant M., Deschamps J., Afik E. and Steinberg V., *Phys. Rev. E* , **85** (2012) 056306.
[15] Finken R., Lamura A., Seifert U. and Gompper G., *Eur. Phys. J. E* , **25** (2008) 309.
[16] Allen M. P. and Tildesley D. J., *Computer Simulation of Liquids* (Clarendon Press, Oxford) 1992.
[17] Malevanets A. and Kapral R., *J. Chem. Phys.* , **110** (1999) 8605.
[18] Kapral R., *Adv. Chem. Phys.* , **140** (2008) 89.
[19] Gompper G., Ihle T., Kroll D. M. and Winkler R. G., *Adv. Polym. Sci.* , **221** (2009) 1.
[20] Noguchi H., Kikuchi N. and Gompper G., *EPL* , **78** (2007) 10005.
[21] Götze I. O., Noguchi H. and Gompper G., *Phys. Rev. E* , **76** (2007) 046705.
[22] Noguchi H. and Gompper G., *Phys. Rev. E* , **78** (2008) 016706.
[23] Lamura A., Gompper G., Ihle T. and Kroll D. M., *Europhys. Lett.* , **56** (2001) 319.
[24] Messlinger S., Schmidt B., Noguchi H. and Gompper G., *Phys. Rev. E* , **80** (2009) 011901.
[25] Tao Y.-G., Götze I. O. and Gompper G., *J. Chem. Phys.* , **128** (2008) 144902.
[26] Belzons M., Blanc R., Bouillot J. L. and Camoin C., *C. R. Acad. Sci., Paris II* , **292** (1981) 939.
[27] Fåhraeus R. and Lindqvist T., *Am. J. Phys.* , **96** (1931) 562.
[28] Skalak R., Keller S. R. and Secomb T. W., *J. Biomech. Eng.* , **103** (1981) 102.
[29] Fedosov D. A., Pan W., Caswell B., Gompper G. and Karniadakis G. E., *Proc. Natl. Acad. Sci. USA* , **108** (2011) 11772.
[30] Gires P. Y., Danker G. and Misbah C., *Phys. Rev. E* , **86** (2012) 011408.
[31] Bagchi P., *Biophys. J.* , **92** (2007) 1858.
[32] Fedosov D. A., Caswell B., Popel A. S. and Karniadakis G. E., *Microcirculation* , **17** (2010) 615.
[33] Freund J. B. and Orescanin M. M., *J. Fluid Mech.* , **671** (2011) 466.
[34] Kim S., Long L. R., Popel A. S., Intaglietta M. and Johnson P. C., *Am. J. Physiol.* , **293** (2007) H1526.